Low-Complexity 3D AoA Positioning for 5G RedCap UEs in Multipath Indoor Factory Environments

Ilya Averin *, Andrey Pudeev, Seunggye Hwang, Hyunsoo Ko

Posted Date: 1 April 2026

doi: 10.20944/preprints202604.0043.v1

Keywords: indoor positioning; 5G RedCap; Angle of Arrival (AoA); antenna arrays; weighted least squares (WLS); spatial covariance matrix; multipath mitigation; indoor factory (InF)

 doi:10.20944/preprints202604.0043.v1

Article

Low-Complexity 3D AoA Positioning for 5G RedCap UEs in Multipath Indoor Factory Environments

Ilya Averin [1,*], Andrey Pudeev [1], Seunggye Hwang [2] and Hyunsoo Ko [2]

[1] LG Electronics Inc, 28, Bolshoy Sampsoniyevskiy Ave, bldg. 2, Saint Petersburg, Russia

[2] LG Electronics Inc, 19, Yangjae-daero 11-gil, Seocho-gu, Seoul, Republic of Korea

* Correspondence: ilya.averin@lge.com

Abstract

The problem of Reduced Capability (RedCap) User Equipment (UE) positioning within indoor 5G networks is addressed. While conventional approaches rely on time-domain ranging, the limited signal bandwidth associated with RedCap devices often prevents these methods from satisfying stringent accuracy requirements. As an alternative, this paper proposes a positioning framework based on Angle-of-Arrival (AoA) measurements. The framework incorporates a low-complexity AoA estimation algorithm derived from the analysis of the spatial covariance matrix. This procedure inherently generates a link quality metric which, alongside the AoA estimate, is utilized for final UE localization. The proposed localization algorithm belongs to the class of Weighted Least Squares (WLS) estimators and provides a unified approach to UE positioning in both 2D and 3D physical space. Simulation results demonstrate the effectiveness of the proposed framework under the challenging high-multipath conditions inherent to 5G indoor deployments.

Keywords: indoor positioning; 5G RedCap; Angle of Arrival (AoA); antenna arrays; weighted least squares (WLS); spatial covariance matrix; multipath mitigation; indoor factory (InF)

1. Introduction

The ongoing evolution of fifth-generation (5G) networks and the subsequent transition to sixth-generation (6G) networks are driven by rising commercial and technical demands. The diverse set of 5G applications is characterized by the well-known triangle formed by Enhanced Mobile Broadband (eMBB), Ultra-Reliable Low Latency Communications (URLLC), and Massive Machine-Type Communications (mMTC). While the primary objective within each group of applications is to maximize communication performance, the capability to perform positioning is of crucial importance for many existing and potential applications.

In the context of 5G communication systems, positioning is a procedure aimed at estimating the unknown coordinates of user equipment (UE), under the assumption that the coordinates of the transmission and reception points (TRPs) are known. The TRPs involved in this process are commonly referred to as reference nodes or anchor points.

A variety of ambitious 5G applications, such as autonomous vehicles, digital twins, and augmented reality can potentially benefit from high-accuracy positioning. Furthermore, access to location-aware services is of great practical interest for a range of industrial segments known as Industry 4.0. For example, highly automated plants may require high-precision positioning for gathering information about resource placement, as well as for tracking assets and tools in both production and storage. As 5G deployments gain momentum, the challenge of 5G positioning and, specifically, indoor positioning, is attracting significant research interest [1,2].

The performance of widespread time-domain positioning methods based on Time of Arrival (ToA) or Time Difference of Arrival (TDoA) estimation is known to be strongly dependent on the signal bandwidth (BW) [2]. While a wide signal BW is inherent to some 5G use cases, this is not always the case. In particular, 3GPP Rel-18 features the positioning of Reduced Capability (RedCap)

 doi:10.20944/preprints202604.0043.v1

UEs [3]. RedCap UEs include wearables (e.g., smartwatches, medical devices, and AR/VR goggles), industrial wireless sensors, and video surveillance. The primary motivation for RedCap UEs is to reduce cost and complexity compared to high-end eMBB and URLLC devices. This requires significant hardware simplification and, more importantly for positioning, a reduction in signal BW. Specifically, the maximum UE bandwidth is 20 MHz for FR1 and 100 MHz for FR2. At the same time, stringent positioning performance must be maintained. For commercial use cases, the horizontal and vertical positioning accuracy should be better than 3 m, while for industrial use cases, the target is under 1 m (horizontal) and 3 m (vertical) for 90% of UEs [4].

Given the bandwidth (BW) limitations, achieving the required positioning accuracy with ToA/TDoA approaches may be challenging. Therefore, alternative methods must be considered. One such approach is based on Angle of Arrival (AoA) measurements [1]. The primary advantage of angular-domain positioning is that its performance is only weakly dependent on the signal BW [5]. A practical drawback of AoA-based methods is the requirement for multiple-antenna systems at the receiver; however, antenna arrays are already widely used for communication and are an inherent part of 5G networks. Furthermore, AoA estimation can be performed on the uplink. Consequently, AoA-based positioning can be implemented for low-cost RedCap UEs equipped with only a single antenna.

In multipath conditions, the accuracy of AoA estimation is known to degrade more severely than that of ToA/TDoA [5]. This can lead to a significant reduction in positioning performance. Since dense multipath environments are inherent to 5G indoor deployments (e.g., the Indoor Factory (InF) scenario [6]), obtaining accurate AoA estimates for RedCap UEs may be challenging. Nevertheless, the high density of TRPs ensures that multiple AoA estimates are potentially available. Consequently, rather than focusing solely on the precision of individual estimates, one can utilize a link quality metric as an indicator of estimation quality. This metric can then be used for selecting or weighting the AoA estimates involved in the positioning process

The main contributions of this paper are as follows:

- Low-Complexity AoA Estimation: A simple algorithm for 1D and 2D Angle of Arrival (AoA) estimation based on the principal eigenvector of the spatial covariance matrix. This method is applicable to both Uniform Linear Arrays (ULAs) and Uniform Rectangular Arrays (URAs).
- Intrinsic Link Quality Metric: A novel metric generated inherently during the AoA estimation process. This metric enables the dynamic weighting of User Equipment (UE)-to-TRP communication links to prioritize reliable measurements in multipath-rich environments.
- Unified Localization Framework: An effective UE localization algorithm utilizing the derived AoA estimates and link quality metrics. Based on the Weighted Least Squares (WLS) estimation framework, it provides a consistent approach for positioning across both 2D and 3D physical spaces.

The effectiveness of the proposed positioning framework in the dense multipath conditions inherent to 5G indoor deployments is demonstrated by the presented simulation results. The findings show that the stringent positioning accuracy requirements for RedCap UEs can be satisfied even in the challenging Indoor Factory (InF) scenario.

2. Positioning Framework

2.1. Motivation for AoA-Based Approach

The most common approach to 5G positioning is based on time-domain ranging [7]. The underlying principle of the ToA method is to measure the propagation delay between transmission and reception, which is subsequently translated into the distance between a transmitter (e.g., the UE) and a receiver (e.g., the TRP). For ToA-based ranging to be effective, the TRP and the UE must be strictly synchronized. This requirement can be relaxed by transitioning to TDoA method, which utilizes the difference in arrival delays between the UE and two or more TRPs. In this scenario, only

 doi:10.20944/preprints202604.0043.v1

the TRPs must be synchronized, which simplifies the practical implementation of the positioning system.

Both ToA and TDoA methods can potentially provide high ranging accuracy, even in the dense multipath conditions inherent to 5G indoor deployments. This accuracy can be further enhanced by utilizing carrier phase (CP) measurements [8]. However, to achieve the extremely high precision offered by CP-based methods, the integer ambiguity problem must be resolved. In general, this requires additional system resources, such as multiple carriers or a greater number of TRPs compared to standard ToA/TDoA approaches.

Once the time delays corresponding to several unique TRP-UE pairs are available, the UE coordinates can be determined by solving a trilateration (or multilateration) problem. This problem has a clear geometric interpretation [9]: for ToA, each delay value defines a sphere centered on the corresponding TRP, while for TDoA, each pair of delay values defines a hyperboloid with foci at the respective TRPs. Ideally, if measurements are error-free, the UE coordinates are located at the intersection of these spheres or hyperboloids. Consequently, trilateration is a fundamentally non-linear problem. While some linearization techniques are possible [9], solving the original non-linear problem can require considerable computational resources.

It is straightforward to see that any timing jitter between reference nodes translates directly into a dilution of precision for TDoA-based positioning. Nevertheless, in the context of 5G networks, the required nanosecond-level time synchronization can be maintained. The fundamental bottleneck of ToA/TDoA-based positioning remains the strong dependency of ranging accuracy on the signal BW [2]. Consequently, positioning performance degrades considerably as the BW decreases. Furthermore, multipath interference is more problematic for narrowband signals, as the signal's temporal characteristics become wide relative to the channel delay spread [5].

Therefore, it is expected that applying time-domain methods to indoor RedCap UEs will result in insufficient positioning accuracy. This challenge can be addressed by alternative approaches that analyze the received signal in either the power or angular domains.

The simplest form of power-based positioning utilizes Received Signal Strength (RSS) measurements to perform power-domain ranging. However, due to the non-linear mapping between signal power and distance, particularly in dense multipath environments, this method typically yields low positioning accuracy. While significantly higher accuracy can be achieved through fingerprinting, such solutions require an extensive offline calibration stage and lack robustness against environmental changes or setup alterations [1].

Angle-based positioning utilizes information regarding the direction from which a signal is received, specifically through AoA measurements. The primary advantage of AoA-based positioning is that estimation accuracy is largely independent of the signal BW. Consequently, AoA-based methods can perform effectively with narrowband or even unmodulated signals [6]. This imposes significantly more relaxed bandwidth requirements compared to ToA, TDoA, and CP techniques. Moreover, AoA-based positioning has less stringent time synchronization requirements than those of time-domain methods [6].

Provided that the AoAs corresponding to several unique TRP-UE pairs are available, the UE coordinates can be determined by solving a triangulation problem. Similar to trilateration, triangulation has a clear geometric interpretation [9]: assuming error-free measurements, the UE coordinates are located at the intersection of rays originating from the respective TRPs. Consequently, unlike trilateration, triangulation can be formulated as a fundamentally linear problem. Furthermore, only two reference points are required to perform AoA-based positioning in 3D space, which offers a significant practical advantage over ToA/TDoA-based methods that require at least four. Accordingly, AoA-based techniques represent a promising alternative for the positioning of RedCap UEs.

Despite its advantages, AoA-based positioning possesses certain limitations. First, a practical drawback is the requirement for specialized hardware to perform AoA estimation. While the field of AoA estimation has been established in radar and other sensing systems for decades, it generally

 doi:10.20944/preprints202604.0043.v1

relies on phase-based methods [10]. This approach evaluates the orientation of the constant-phase wavefront and can be implemented in various ways. For example, AoA can be estimated by rotating a directional antenna; in this case, the AoA estimate corresponds to the direction where the RSS is maximized or minimized.

With advancements in digital signal processing, another phase-based approach known as spatial aperture sampling [10] has seen widespread adoption. While this can take various forms, it is most commonly implemented using antenna arrays. To ensure accurate AoA estimation, these arrays must be calibrated following installation and periodically maintained to minimize measurement uncertainty. Nevertheless, given that antenna arrays are already extensively utilized in 5G systems for communication, their reuse for positioning provides a significant added benefit. Furthermore, by performing positioning on the uplink, all complex processing and hardware requirements are shifted to the TRPs. This allows low-cost RedCap UEs to remain simple, requiring only a single antenna.

A more fundamental drawback of AoA-based positioning is that its accuracy is determined by both the precision of the AoA estimate and the distance between the TRP and the UE. This stands in contrast to ToA/TDoA methods, where ranging accuracy depends primarily on the precision of the delay measurements. While this distance dependency can be a limiting factor in outdoor positioning, the indoor environment typically involves much shorter TRP-to-UE distances. Consequently, provided the AoA estimation is sufficiently accurate, high positioning precision can be achieved. This suggests that the bottleneck for such systems lies primarily in the accuracy of the AoA estimation itself.

Numerous AoA estimation methods for antenna arrays have been presented in the literature. The beamformer developed by Bartlett [11] is widely considered a reference technique, known for its effectiveness and robustness against hardware impairments. However, its performance can significantly degrade in the dense multipath conditions inherent to indoor deployments. This degradation is primarily caused by wavefront distortion, which occurs when multiple replicas of the transmitted signal arrive at the receiver from closely spaced angles.

To address this challenge, one may apply super-resolution techniques, such as Capon's algorithm [12] or subspace-based methods like MUSIC [13] and ESPRIT [14]. Other notable techniques include the Maximum Likelihood (ML) estimator [15] and the computationally efficient Root-MUSIC algorithm [16]. While these methods can provide superior AoA estimation accuracy, they often require significant computational resources. Furthermore, super-resolution algorithms are known to be sensitive to hardware impairments [17]. Beyond these factors, the number of antenna elements imposes a fundamental limit on the maximum number of resolvable paths, which may significantly degrade performance in dense multipath environments.

As an alternative strategy, rather than focusing on resolving individual multipath components to enhance AoA estimation accuracy, one can incorporate a quality indicator for the AoA estimates. Such an indicator enables the ranking and weighting of AoA measurements used for localization. Provided the TRP density is sufficiently high and an adequate number of AoA estimates is available, the target positioning performance can be attained even with a low-complexity estimation method.

2.2. Positioning in 2D Space

2.2.1. 1D AoA Estimation

Assume a TRP is equipped with an ULA consisting of N identical isotropic elements with uniform inter-element spacing d (Figure 1). Let J be the number of narrowband plane waves, centered at a carrier frequency f_c (with a corresponding wavelength λ_c), impinging on the array from directions $\{\theta_1, \theta_2, \ldots, \theta_J\}$. The *ith* wave is associated with the *ith* of J signal sources whose AoA is denoted as θ_i. As illustrated in Figure 1, the AoA is defined as the angle between the broadside of the array (the line orthogonal to the array axis) and the direction of the impinging wave's propagation.

 doi:10.20944/preprints202604.0043.v1

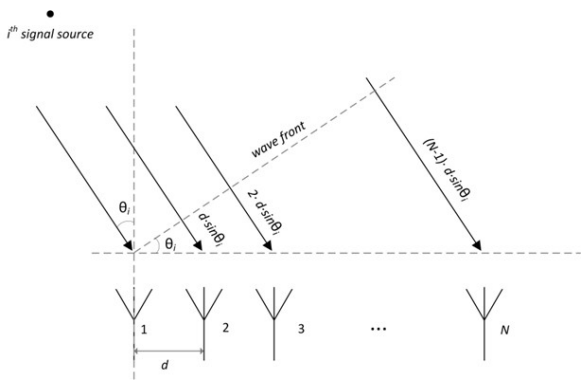

Figure 1. 2D signal model and geometric configuration of the antenna array.

The response of the antenna array to a plane wave impinging at an angle θ is defined by the steering vector [18]. Accordingly, we define the $N\times J$ steering matrix, $\mathbf{\Phi}$, whose columns are the steering vectors for angles $\{\theta_1, \theta_2, \dots, \theta_J\}$:

$$\mathbf{\Phi} = \left[\mathbf{F}(\theta_1)\ \mathbf{F}(\theta_2)\ \dots\ \mathbf{F}(\theta_J)\right] \tag{1}$$

It is apparent that the steering matrix $\mathbf{\Phi}$ characterizes the information regarding the angular positions of the signal sources. Consequently, by identifying the components of $\mathbf{\Phi}$, one can derive the estimates of the AoAs.

In the case of a ULA, the steering vector takes the following simple form:

$$\mathbf{F}(\theta_i) = \left[1\ e^{-jk_i}\ e^{-j2k_i}\ \dots\ e^{-j(N-1)k_i}\right]^T \tag{2}$$

where the superscript 'T' indicates the transpose. The parameter k_i is defined as:

$$k_i = \frac{2\pi d}{\lambda_c}\sin\theta_i = 2\pi d_\lambda \sin\theta_i \tag{3}$$

where d_λ represents the normalized inter-element spacing in units of wavelength.

Assuming the *ith* source corresponds to the received signal $s_i(t)$, the array output vector can be expressed as:

$$\mathbf{X}(t) = \mathbf{\Phi}\mathbf{S}(t) + \mathbf{N}(t) \tag{4}$$

where $\mathbf{S}(t) = \left[s_1(t)\ s_2(t)\ \dots\ s_J(t)\right]^T$ is the signal vector and $\mathbf{N}(t) = [n_1(t)\ n_2(t)\ \dots\ n_N(t)]^T$ is the additive noise vector.

Based on this model, the spatial covariance matrix of the received signal vector can be defined as:

$$\mathbf{M} = \mathbb{E}\{\mathbf{X}(t)\mathbf{X}(t)^H\} \tag{5}$$

where $\mathbb{E}\{\cdot\}$ denotes the expectation operator and the superscript 'H' indicates the Hermitian transpose.

Under the assumption that the noise is spatially white and uncorrelated with the signals, it follows from (5) that

$$\mathbf{M} = \mathbf{\Phi}\mathbf{P}\mathbf{\Phi}^H + \sigma^2\mathbf{I} \tag{6}$$

where σ^2 is the noise variance, $\mathbf{I}$ is the $N\times N$ identity matrix. The $J\times J$ matrix $\mathbf{P}$ represents the source covariance matrix, defined as:

$$\mathbf{P} = \mathbb{E}\{\mathbf{S}(t)\mathbf{S}(t)^H\} \tag{7}$$

The *ith* diagonal element of matrix $\mathbf{P}$ represents the power of the signal $s_i(t)$. In the event that the received signals are pairwise uncorrelated, $\mathbf{P}$ becomes a diagonal matrix.

 doi:10.20944/preprints202604.0043.v1

Being a Hermitian matrix, the spatial covariance matrix $\mathbf{M}$ can be represented by its spectral decomposition:

$$\mathbf{M} = \sum_{i=1}^{N} \lambda_i \mathbf{U}_i \mathbf{U}_i^H \tag{8}$$

where λ_i is the *ith* eigenvalue and $\mathbf{U}_i$ is the corresponding *ith* eigenvector of the matrix $\mathbf{M}$.

If the number of antenna elements exceeds the number of signals (i.e., $N>J$) and the steering matrix is of full rank, the spectral decomposition in (8) can be partitioned into two distinct components. The first part consists of eigenvectors corresponding to eigenvalues equal to the noise variance, thereby spanning the noise subspace. The second part corresponds to the remaining J larger eigenvalues, which span the signal subspace:

$$\mathbf{M} = \mathbf{E}_s \mathbf{\Lambda}_s \mathbf{E}_s^H + \sigma^2 \mathbf{E}_n \mathbf{E}_n^H \tag{9}$$

where $\mathbf{E}_s = [\mathbf{U}_1, \mathbf{U}_2, \ldots \mathbf{U}_J]$ and $\mathbf{E}_n = [\mathbf{U}_{J+1}, \mathbf{U}_{J+2}, \ldots \mathbf{U}_N]$ are the matrices, whose columns consist of the signal and noise eigenvectors, respectively. The $J \times J$ matrix $\mathbf{\Lambda}_s = \mathrm{diag}[\lambda_1, \lambda_2, \ldots \lambda_J]$ is the diagonal matrix containing the corresponding signal eigenvalues.

By exploiting the orthonormality of the eigenvectors, Equation (9) can be transformed into:

$$\mathbf{M} = \mathbf{E}_s(\mathbf{\Lambda}_s - \sigma^2)\mathbf{E}_s^H + \sigma^2 \mathbf{I} \tag{10}$$

In the case where only a single source exists (i.e., J=1), Equation (6) reduces to:

$$\mathbf{M} = p\mathbf{F}(\theta_1)\mathbf{F}(\theta_1)^H + \sigma^2 \mathbf{I} \tag{11}$$

where p represents the power of the signal $s_1(t)$. Furthermore, Equation **Error! Reference source not found.** can be simplified as follows:

$$\mathbf{M} = (\lambda_1 - \sigma^2)\mathbf{U}_1 \mathbf{U}_1^H + \sigma^2 \mathbf{I} \tag{12}$$

where λ_1 is the signal eigenvalue and $\mathbf{U}_1$ is the corresponding eigenvector.

By comparing (11) and (12), it can be concluded that in the single-source case, the steering vector $\mathbf{F}(\theta_1)$ and the principal eigenvector $\mathbf{U}_1$ of the spatial covariance matrix $\mathbf{M}$ coincide, differing only by a scaling factor. Since eigenvectors are defined with a unit L^2-norm and considering the structure of the steering vector in (2) and (3), the relationship can be expressed as:

$$\mathbf{U}_1 = \frac{1}{\sqrt{\mathrm{N}}}\mathbf{F}(\theta_1) = \frac{1}{\sqrt{\mathrm{N}}}\begin{bmatrix} 1 \\ e^{-j2\pi d_\lambda \sin\theta_1} \\ \ldots \\ e^{-j2\pi(i-1)d_\lambda \sin\theta_1} \\ \ldots \\ e^{-j2\pi(N-1)d_\lambda \sin\theta_1} \end{bmatrix} \tag{13}$$

It is straightforward to see from (13) that the phase difference Δ between any two adjacent elements of the eigenvector $\mathbf{U}_1$ is given by:

$$\Delta = \angle(\mathbf{U}_{1_i}) - \angle(\mathbf{U}_{1_{i-1}}) = \varphi_i - \varphi_{i-1} = -2\pi d_\lambda \sin\theta_1 \tag{14}$$

where $\mathbf{U}_{1_i}$ denotes the *ith* element of $\mathbf{U}_1$ and φ_i is its corresponding phase.

Thus, the locus of $\angle(\mathbf{U}_{1_i})$ is a straight line with a slope equal to Δ (represented by the dashed line in Figure 2). Based on this relationship, the estimate for the AoA $\hat{\theta}_1$ is directly obtained as:

$$\hat{\theta}_1 = -\sin^{-1}\left(\frac{\Delta}{2\pi d_\lambda}\right) \tag{15}$$

 doi:10.20944/preprints202604.0043.v1

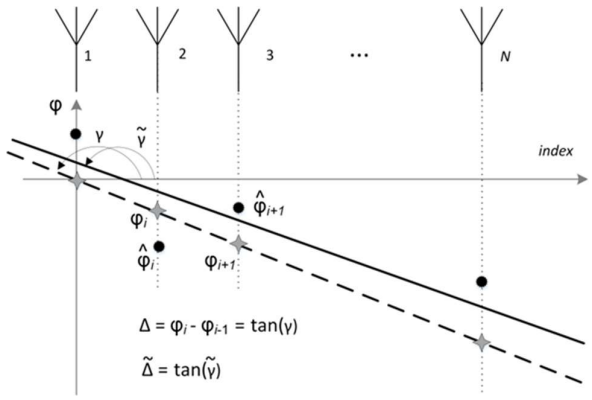

Figure 2. Phase progression of the principal eigenvector elements for the ideal Line-of-Sight (LoS) case (J=1, stars) and the multipath scenario (J>1, filled circles).

As follows from (15), the obtained AoA estimate is inherently ambiguous. The maximum angular support provided by a ULA with isotropic elements is limited to a semi-plane, i.e., $\hat{\theta}_1 \in [-\pi/2, \pi/2]$ provided that $d_\lambda \leq 0.5$. In practice, however, this ambiguity can be readily resolved, for example, by utilizing non-isotropic elements with specific radiation patterns.

A more fundamental challenge is that (15) is valid only for the single-source case. In a communications context, this implies ideal Line-of-Sight (LoS) conditions, which assume the absence of multipath propagation. Such conditions are improbable for the majority of 5G deployments, particularly in Indoor Factory (InF) scenarios. Conversely, under more realistic LoS-plus-multipath conditions, one may expect a considerable number of indirect paths, each acting as a distinct signal source. Each of these sources contributes a corresponding signal eigenvalue and signal eigenvector to the spatial covariance matrix.

Assuming the direct path yields the strongest signal, it corresponds to the largest eigenvalue. The related signal eigenvector is defined as the principal eigenvector $\mathbf{U}_s$. It can be shown that, provided the sources are uncorrelated, any signal eigenvector is a linear combination of the steering vectors. Consequently, the locus of $\angle(\mathbf{U}_{s_i})$ deviates from a straight line, and equality (15) no longer holds.

Nevertheless, one can identify the principal eigenvector $\mathbf{U}_s$ of the spatial covariance matrix $\mathbf{M}$ and approximate its phase progression with a straight line (represented by the solid line in Figure 2). This is achieved by formulating the task as a linear regression problem. In other words, a functional dependent on two parameters (representing the slope and the intercept) must be minimized:

$$f(\tilde{\Delta}, \beta) = \min\left\{\sum_{i=1}^{N} (\hat{\varphi}_i - \tilde{\varphi}_i)^2\right\} = \min\left\{\sum_{i=1}^{N} \varepsilon_i^2\right\} = \min\{\|\mathbf{E}\|^2\} \tag{16}$$

where $\hat{\varphi}_i$ represents the phase of the *ith* element of principal eigenvector $\mathbf{U}_s$ and $\tilde{\varphi}_i$ is the corresponding phase value derived from the linear approximation. The operator $\|\cdot\|$ denotes the L^2-norm and $\mathbf{E}$ is the residual error vector composed of the individual approximation errors ε_i.

The functional in (16) reaches its minimum for the parameter vector:

$$\begin{bmatrix}\tilde{\Delta} \\ \beta\end{bmatrix} = (\mathbf{C}^T\mathbf{C})^{-1}\mathbf{C}^T \begin{bmatrix}\hat{\varphi}_1 \\ \hat{\varphi}_2 \\ \dots \\ \hat{\varphi}_N\end{bmatrix} \tag{17}$$

where the observation matrix $\mathbf{C}$ is defined as:

$$\mathbf{C} = \begin{bmatrix}1 & 1 \\ 2 & 1 \\ \dots & \dots \\ N & 1\end{bmatrix} \tag{18}$$

 doi:10.20944/preprints202604.0043.v1

By replacing the slope Δ in (15) with its approximation $\widetilde{\Delta}$ derived from (17), the required estimate for the LoS AoA is obtained as:

$$\hat{\theta}_{LoS} = -\sin^{-1}\left(\frac{\widetilde{\Delta}}{2\pi d_{\lambda}}\right) \tag{19}$$

Equation (19) provides a low-complexity method for 1D AoA estimation in the presence of multipath. Similar to the Bartlett beamformer, this estimator lacks super-resolution capability; however, it naturally yields a quality indicator for the AoA estimate, or more concisely, a link quality metric.

It is straightforward to see that the AoA estimate provided by the proposed algorithm coincides with the true AoA under ideal LoS conditions. In such a case, the residual approximation errors ε_i are zero, and the functional in (16) reaches its absolute minimum of zero. Consequently, the L^2-norm of the error vector $\mathbf{E}$ serves as an indicator of how closely the UE-to-TRP communication link approximates the favorable propagation conditions required for high-quality AoA estimation.

It follows from (16) and (17) that the residual error vector $\mathbf{E}$ can be expressed as:

$$\mathbf{E} = \begin{bmatrix} \widehat{\varphi}_1 \\ \widehat{\varphi}_2 \\ \dots \\ \widehat{\varphi}_N \end{bmatrix} - \mathbf{C}\begin{bmatrix} \widetilde{\Delta} \\ \beta \end{bmatrix} \tag{20}$$

Considering that the number of antenna elements affects the L^2-norm of vector $\mathbf{E}$ and to account for the variability in antenna array configurations, it is appropriate to define the link quality metric as the normalized norm:

$$\chi = \sqrt{\frac{1}{N}\sum_{i=1}^{N}\varepsilon_i^2} = \frac{\|\mathbf{E}\|}{\sqrt{N}} \tag{21}$$

where χ represents the Root Mean Square (RMS) phase error across the array.

It should be emphasized that (5) defines the true spatial covariance matrix, assuming it is perfectly known. In practice, however, the true matrix is unavailable, and one must operate with an estimate. Numerous approaches exist for estimating the spatial covariance matrix, including adaptations for correlated sources [16,19–21]. These methods typically derive the estimate from a finite number of time-domain snapshots. A straightforward yet effective approach is to utilize the sample covariance matrix, $\widehat{\mathbf{M}}$, which represents the unstructured maximum likelihood estimate of the spatial covariance matrix.

Since 5G NR utilizes OFDM signals, frequency-domain channel estimation is typically more practical than time-domain methods [22]. In practice, the spatial covariance matrix is estimated using a finite number of channel estimates obtained from a set of pilot subcarriers. Analogous to the time-domain approach, the frequency-domain sample covariance matrix can be employed as the spatial covariance estimate:

$$\widehat{\mathbf{M}} = \mathrm{diag}\left(\widetilde{\mathbf{M}}\right)^{-1/2}\widetilde{\mathbf{M}}\,\mathrm{diag}\left(\widetilde{\mathbf{M}}\right)^{-1/2} \tag{22}$$

where $\widetilde{\mathbf{M}}$ is the unnormalized sample covariance matrix defined as:

$$\widetilde{\mathbf{M}} = \frac{1}{L}\sum_{l=1}^{L}\widehat{\boldsymbol{h}}(l)\widehat{\boldsymbol{h}}(l)^H \tag{23}$$

In these expressions, L denotes the number of pilot subcarriers used for channel estimation and $\widehat{\boldsymbol{h}}(l)$ is the $N\times1$ channel estimate vector across N receiving antennas.

Consequently, to perform AoA estimation, specifically to apply the estimator (19) and derive the link quality metric (21), the principal eigenvector of the true spatial covariance matrix is replaced by the corresponding eigenvector of the sample covariance matrix $\widetilde{\mathbf{M}}$ defined in (22).

 doi:10.20944/preprints202604.0043.v1

2.2.2. UE Localization

Assume that positioning is performed using *K* TRPs with known coordinates. In the 2D space under consideration, the position of the *pth* TRP is defined by the coordinates (x_p, y_p). These *K* UE-to-TRP links provide a set of AoA estimates, $\{\hat{\theta}_p\}$, which are defined within a global coordinate system. The objective is to estimate the UE coordinates in 2D space, denoted as $(\hat{x}_o, \hat{y}_o)$.

It is important to note that the AoA estimate (19) is defined within the local coordinate system of the specific antenna array. Therefore, to transform this estimate into the global coordinate system, the orientation of each antenna array is assumed to be precisely known.

It is straightforward to see that each AoA estimate defines a straight line passing through the coordinates of both the TRP and the UE. Under the assumption of perfect AoA estimation, the unique intersection of these *K* lines determines the UE position, $(\hat{x}_o, \hat{y}_o)$, as illustrated in Figure 3a.

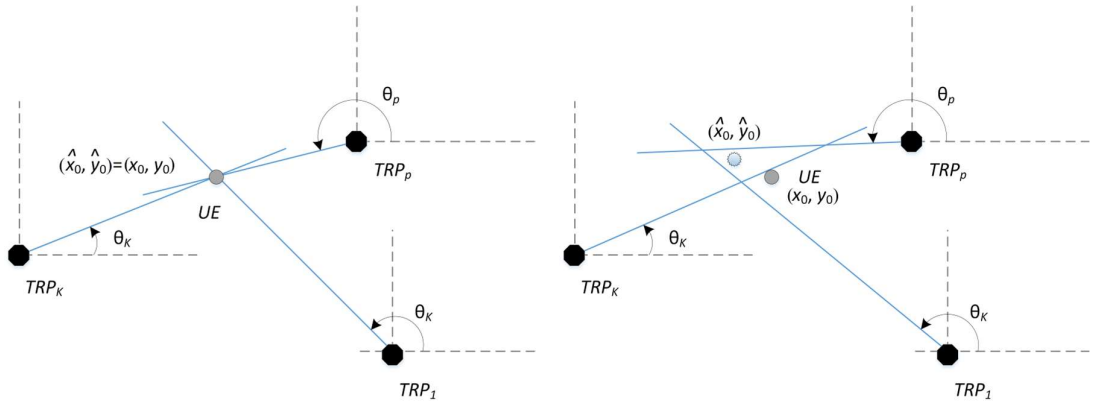

(**a**) (**b**)

Figure 3. 2D AoA-based positioning geometry: (**a**) ideal scenario with error-free angular estimates; (**b**) practical scenario in the presence of estimation errors.

Using the point-slope form of a linear equation, the relationship for the *pth* UE-to-TRP link can be expressed as:

$$y - y_p = a_p(x - x_p) \tag{24}$$

where $a_p = \tan\hat{\theta}_p$ represents the slope of the line determined by the estimated AoA.

Expression (24) facilitates the construction of a system of *K* linear equations:

$$\begin{cases} y = a_1 x + (y_1 - a_1 x_1) \\ \dots \\ y = a_p x + (y_p - a_p x_p) \\ \dots \\ y = a_K x + (y_K - a_K x_K) \end{cases} \tag{25}$$

Alternatively, this system can be expressed in the following matrix form:

$$\begin{bmatrix} -a_1 & 1 \\ -a_2 & 1 \\ \dots & \dots \\ -a_K & 1 \end{bmatrix} \begin{bmatrix} x_0 \\ y_0 \end{bmatrix} = \begin{bmatrix} y_1 - a_1 x_1 \\ y_2 - a_2 x_2 \\ \dots \\ y_K - a_K x_K \end{bmatrix} \Leftrightarrow \mathbf{A} \begin{bmatrix} x_0 \\ y_0 \end{bmatrix} = \mathbf{b} \tag{26}$$

If only two TRPs are available (*K*=2), the system in (25) consists of two equations and yields a single unique solution, provided the equations are consistent. This implies that, theoretically, AoA-based positioning can be performed using only two TRPs. For *K*>2, the system in (25) becomes an overdetermined system of linear equations. In general, such a system has no exact solution due to measurement noise and multipath.

 doi:10.20944/preprints202604.0043.v1

However, assuming that matrix **A** is of full rank, an approximate solution can be derived using the Moore–Penrose pseudoinverse, which corresponds to the Ordinary Least Squares (OLS) estimator [23]:

$$\begin{bmatrix}\hat{x}_o\\ \hat{y}_o\end{bmatrix} = (\mathbf{A}^T\mathbf{A})^{-1}\boldsymbol{A}^T\mathbf{b} \tag{27}$$

In the case where all AoAs are estimated perfectly (i.e., the error-free scenario), the solution provided by (27) coincides with the true UE position, as illustrated in Figure 3a. In practice, however, the accuracy of AoA estimation is finite. Consequently, the position estimate deviates from the true UE coordinates, resulting in a positioning error (see Figure 3b). Generally, this positioning error depends on both the AoA estimation accuracy and the TRP deployment geometry, the latter of which is characterized by the Geometric Dilution of Precision (GDOP).

The primary drawback of the OLS estimator (27) is that it does not incorporate information regarding the quality of the AoA estimates. To address this, one can apply additional conditioning to the available estimates based on the link quality metric (21). While a rigid link selection achieved by selecting a subset of the 'best' links (those corresponding to the smallest metric values) out of the *K* available links is possible, a soft link selection approach is generally superior. This is realized by incorporating a weighting matrix into the LS estimator, which provides a more optimal and robust solution.

Following this strategy, the UE position estimate can be determined using the Weighted Least Squares (WLS) estimator:

$$\begin{bmatrix}\hat{x}_o\\ \hat{y}_o\end{bmatrix} = (\mathbf{A}^T\mathbf{W}\mathbf{A})^{-1}\mathbf{A}^T\mathbf{W}\mathbf{b} \tag{28}$$

where the *K*x*K* weighting matrix **W** is a diagonal matrix defined as:

$$\mathbf{W} = \frac{1}{\sum_{p=1}^{K}\chi_p^{-2}}\begin{bmatrix}\chi_1^{-2} & 0 & \dots & 0\\ 0 & \chi_2^{-2} & \dots & 0\\ \dots & \dots & \dots & 0\\ 0 & 0 & 0 & \chi_K^{-2}\end{bmatrix} \tag{29}$$

In this expression, χ_p represents the link quality metric of the *pth* UE-to-TRP link, calculated according to (21).

2.3. Positioning in 3D Space

2.3.1. 2D AoA Estimation

The 2D positioning problem discussed previously relies on 1D AoA estimation. In contrast, positioning in 3D physical space necessitates 2D AoA estimation, requiring the simultaneous estimation of both the azimuth angle θ_i and the zenith angle ψ_i (see Figure 4). It is important to highlight that the 2D AoA estimation problem can be decoupled into two independent 1D AoA estimation tasks. Specifically, the azimuth and zenith angles can be estimated separately by exploiting the orthogonal geometry of the antenna array.

While various antenna configurations exist, it is appropriate to generalize the ULA concept by considering a Uniform Rectangular Array (URA). In this case, the 1D AoA estimation results presented in Section 2.2 remain applicable, requiring only minor modifications to accommodate the two-dimensional spatial sampling.

Assume a TRP is equipped with a URA consisting of *N* identical isotropic elements with an inter-element spacing d_H in the horizontal plane, and *M* identical isotropic elements with an inter-element spacing d_V in the vertical plane (see Figure 4). It is evident that the URA comprises of *M*×*N* elements, organized into *M* rows and *N* columns.

Each row and column of the URA can be treated as a separate horizontal or vertical ULA. Consequently, the horizontal spatial covariance matrix can be estimated by averaging the sample covariance matrices across all *M* rows. Using Equation (23), this is expressed as:

 doi:10.20944/preprints202604.0043.v1

$$\widetilde{\mathbf{M}}_H = \frac{1}{M}\sum_{i=1}^{M}\widetilde{\mathbf{M}}_i = \frac{1}{M}\sum_{i=1}^{M}\left\{\frac{1}{L}\sum_{l=1}^{L}\widehat{\boldsymbol{h}}_i(l)\widehat{\boldsymbol{h}}_i(l)^H\right\} \tag{30}$$

where L denotes the number of subcarriers utilized for channel estimation and $\widehat{\boldsymbol{h}}_i(l)$ is the Nx1 channel estimate vector for the *ith* antenna row.

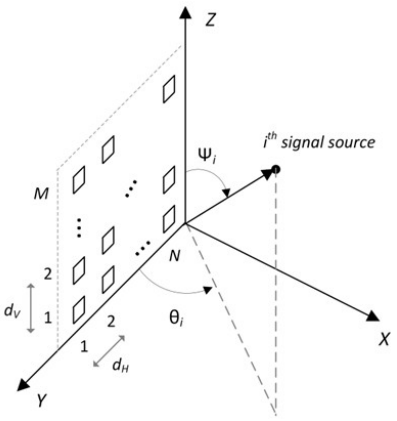

Figure 4. 3D signal model and geometric configuration of the uniform rectangular array (URA).

Similarly, the spatial covariance matrix for the vertical plane can be estimated by averaging the sample covariance matrices across all N columns:

$$\widetilde{\mathbf{M}}_V = \frac{1}{N}\sum_{j=1}^{N}\widetilde{\mathbf{M}}_j = \frac{1}{N}\sum_{i=1}^{N}\left\{\frac{1}{L}\sum_{l=1}^{L}\widehat{\boldsymbol{h}}_j(l)\widehat{\boldsymbol{h}}_j(l)^H\right\} \tag{31}$$

where $\widehat{\boldsymbol{h}}_j(l)$ is the Mx1 vector channel estimate vector for the *jth* antenna column.

By applying the results of Section 2.2.1 to the spatial covariance matrices (30) and (31), the estimates for the azimuth angle $\hat{\theta}_{LoS}$ and the zenith angle $\hat{\psi}_{LoS}$ can be obtained as follows:

$$\hat{\theta}_{LoS} = -\sin^{-1}\left(\frac{\widetilde{\Delta}_{\mathrm{H}}}{2\pi d_{\lambda H}}\right) \tag{32}$$

$$\hat{\psi}_{LoS} = -\sin^{-1}\left(\frac{\widetilde{\Delta}_{\mathrm{V}}}{2\pi d_{\lambda V}}\right) \tag{33}$$

where $\widetilde{\Delta}_H$ and $\widetilde{\Delta}_V$ are the slopes derived from the linear approximation of the phase progression of the principal eigenvectors of matrices $\widetilde{\mathbf{M}}_H$ and $\widetilde{\mathbf{M}}_V$, respectively.

In addition to the 2D AoA estimates, the link quality metrics can be readily determined for both the horizontal and vertical planes:

$$\chi_H = \frac{\|\mathbf{E}_H\|}{\sqrt{N}} \tag{34}$$

$$\chi_V = \frac{\|\mathbf{E}_V\|}{\sqrt{\mathrm{M}}} \tag{35}$$

where $\mathbf{E}_H$ and $\mathbf{E}_V$ are the residual error vectors derived from the linear phase approximations in the horizontal and vertical dimensions, respectively.

In practice, it is beneficial to utilize a single metric to reflect the overall link quality. Such a metric can be obtained by combining (34) and (35). By simply aggregating the individual components, the total link quality metric χ_Σ is defined as:

$$\chi_\Sigma = \chi_H + \chi_V \tag{36}$$

 doi:10.20944/preprints202604.0043.v1

Consequently, the implementation of 2D AoA estimation involves constructing the spatial covariance matrices (30) and (31), extracting their principal eigenvectors, and subsequently applying the estimators in (32) and (33). The link quality metric (36) is obtained as an intrinsic part of this estimation procedure.

2.3.2. UE Localization

Assume that positioning is performed using K TRPs with known coordinates. In the 3D space under consideration, the position of the pth TRP is defined by the coordinates (x_p, y_p, z_p). These K UE-to-TRP links provide a set of 2D AoA estimates, $\{\hat{\theta}_p, \hat{\psi}_p\}$, which are defined within a global coordinate system. The objective is to estimate the UE coordinates in 3D space, denoted as $(\hat{x}_o, \hat{y}_o, \hat{z}_o)$.

The UE coordinates $(\hat{x}_o, \hat{y}_o, \hat{z}_o)$ can be estimated using several approaches. One method involves decoupling the 3D problem into two 2D tasks; for example, by considering the XY and XZ planes separately to solve for the coordinate pairs $(\hat{x}_o, \hat{y}_o)$ and $(\hat{x}_o, \hat{z}_o)$. Alternatively, a successive estimation approach can be employed where the horizontal coordinates $(\hat{x}_o, \hat{y}_o)$ are determined in the first step. Given the known TRP positions and the available zenith angle estimates, the vertical coordinate $\hat{z}_o$ can then be directly recovered for each UE-to-TRP link.

Nevertheless, the 3D positioning problem can be addressed using a unified approach based on the generalized parametric representation of a straight line in $\mathbb{R}^3$. By leveraging projective geometry and the WLS framework, the 3D UE position can be estimated as [24]:

$$\begin{bmatrix} \hat{x}_o \\ \hat{y}_o \\ \hat{z}_o \end{bmatrix} = \left(\sum_{p=1}^{K} \mathbf{W}_p \mathbf{U}_p^{\perp} \right)^{-1} \sum_{p=1}^{K} \mathbf{W}_p \mathbf{U}_p^{\perp} \begin{bmatrix} x_p \\ y_p \\ z_p \end{bmatrix} \tag{37}$$

where $\mathbf{W}_p$ is the 3×3 weighting matrix for the pth UE-to-TRP link and $\mathbf{U}_p^{\perp} = \mathbf{I} - \mathbf{u}_p \mathbf{u}_p^T$ is the 3×3 rank-2 symmetric idempotent projection matrix. This matrix projects any vector onto the plane orthogonal to the unit direction vector $\mathbf{u}_p$. The vector $\mathbf{u}_p$ is determined by the 2D AoA estimate $\{\hat{\theta}_p, \hat{\psi}_p\}$ as follows:

$$\mathbf{u}_p = \begin{bmatrix} \cos\hat{\theta}_p \sin\hat{\psi}_p \\ \sin\hat{\theta}_p \sin\hat{\psi}_p \\ \cos\hat{\psi}_p \end{bmatrix} \tag{38}$$

The solution (37) can be efficiently implemented using a block-matrix representation:

$$\begin{bmatrix} \hat{x}_o \\ \hat{y}_o \\ \hat{z}_o \end{bmatrix} = \left(\mathbf{U}^{\perp T} \mathbf{W} \mathbf{U}^{\perp} \right)^{-1} \mathbf{U}^{\perp T} \mathbf{W} \boldsymbol{\rho} \tag{39}$$

where matrix $\mathbf{U}^{\perp}$ is a $3K$×3 matrix composed of the individual projection matrices $\mathbf{U}_p^{\perp}$:

$$\mathbf{U}^{\perp} = \begin{bmatrix} \mathbf{U}_1^{\perp} \\ \dots \\ \mathbf{U}_K^{\perp} \end{bmatrix} \tag{40}$$

The $3K$×$3K$ block diagonal matrix $\mathbf{W}$ consists of K symmetric positive-definite weighting matrices:

$$\mathbf{W} = \begin{bmatrix} \mathbf{W}_1 & 0 & \dots & 0 \\ 0 & \mathbf{W}_2 & \dots & \dots \\ \dots & \dots & \dots & \dots \\ 0 & \dots & \dots & \mathbf{W}_K \end{bmatrix} \tag{41}$$

and the $3K$×1 vector $\boldsymbol{\rho}$ is formed by the concatenated coordinates of the TRPs:

 doi:10.20944/preprints202604.0043.v1

$$\boldsymbol{\rho} = \begin{bmatrix} \begin{bmatrix} x_1 \\ y_1 \\ z_1 \end{bmatrix} \\ \cdots \\ \begin{bmatrix} x_K \\ y_K \\ z_K \end{bmatrix} \end{bmatrix} \tag{42}$$

It is evident that while the WLS estimator (39) requires a 3×3 weighting matrix for each UE-to-TRP link, the link quality metric derived in (36) is a scalar value. To satisfy this requirement, the weighting matrix for the *pth* link can be defined as:

$$\mathbf{W}_p = \frac{1}{\sum_{p=1}^{K} \chi_{\Sigma_p}^{-2}} \begin{bmatrix} \chi_{\Sigma_p}^{-2} & 0 & 0 \\ 0 & \chi_{\Sigma_p}^{-2} & 0 \\ 0 & 0 & \chi_{\Sigma_p}^{-2} \end{bmatrix} \tag{43}$$

It is important to note that AoA estimation accuracy often depends on the value of the true AoA. Generally, peak estimation performance is achieved when the incident signal aligns with the antenna array boresight. Consequently, as the azimuth approaches $\pm\pi/2$ (the array end-fire), the precision of the AoA estimates typically degrades. In practice, it is therefore effective to perform pre-filtering of the metrics used in (43) based on their angular values. Given a set of K available links, one can select only those whose AoA estimates fall within a specified angular support interval. This pre-filtering approach can be formulated as:

$$\chi_{\Sigma_l} = \chi_{\Sigma_p}\Big|_{\substack{|\hat{\theta}_p| \le T_r, \\ |\hat{\psi}_p| \le T_r}} \tag{44}$$

where T_r is the angular threshold defining the reliable estimation range.

3. Experiment and Result Analysis

3.1. Positioning in 2D Space

The simulation results evaluating the performance of the proposed positioning method are presented in Figure 5. These results correspond to the InF-SH scenario [6], utilizing a 5 MHz signal bandwidth with all TRPs and UEs located at a uniform height, consistent with the 2D positioning model described in Section 2.2. The UEs are assumed to be uniformly distributed throughout the horizontal plane. Each TRP is equipped with a ULA consisting of N = 8 identical isotropic elements with an inter-element spacing of $d_\lambda = 0.5$, while the UE utilizes a single isotropic antenna. The transmit power is set to 23 dBm.

The 1D AoA estimation is performed on the uplink using the estimator (19). The positioning is derived from either the OLS (27) or WLS (28) estimators, incorporating the link quality metric provided by (21). The positioning error is defined as the Euclidean distance between the true and estimated UE coordinates.

In the InF-SH scenario, 18 TRPs are arranged in a regular grid within a rectangular area, providing a maximum of K = 18 reference points for positioning. As illustrated in Figure 5, the positioning accuracy achieved using the OLS estimator with all available links is notably poor (blue curve). In the absence of link quality information, one might attempt to improve results by randomly selecting a subset of links (e.g., K = 3). However, this approach yields only a marginal improvement in accuracy (brown curve).

The availability of the link quality metric enables significant improvements in positioning accuracy through link selection. By applying a rigid link selection strategy, one can choose the K best links (e.g., K = 4) from the total set of 18 and calculate the OLS solution (red curve, Figure 5). It is evident that this approach substantially enhances accuracy compared to random selection. However, employing the WLS estimator (28), which acts as a soft link selection mechanism, on the full set of 18 links yields even better performance (black curve). Specifically, the 90*th* percentile of the positioning error is reduced to 1.45 m.

 doi:10.20944/preprints202604.0043.v1

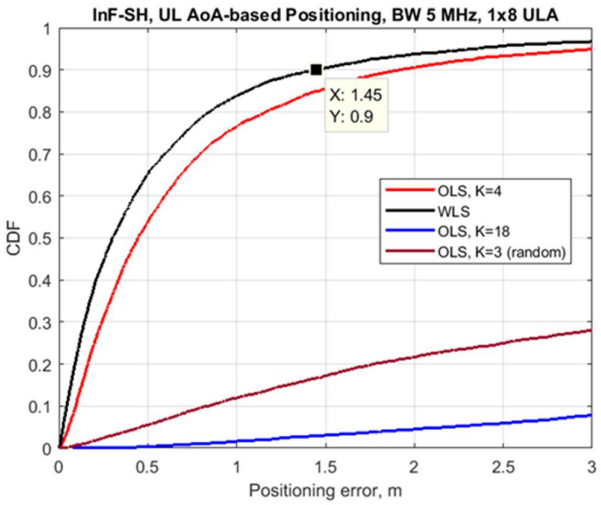

Figure 5. CDF of the positioning error for the 2D InF-SH scenario (5 MHz bandwidth, 1x8 ULA).

3.2. Positioning in 3D Space

The simulation results evaluating the performance of the proposed 3D positioning method are presented in Figure 6. The figure illustrates the horizontal positioning accuracy for the InF-SH scenario utilizing a 5 MHz signal bandwidth. In this setup, all TRPs are deployed at a uniform height of 8 m, while the UEs are distributed throughout the horizontal plane at a constant height of 1.5 m. Each TRP is equipped with a URA consisting of $M \times N$ elements ($M = N = 8$) with identical inter-element spacings of $d_{\lambda H} = d_{\lambda V} = 0.5$. The UE utilizes a single isotropic antenna and the transmit power is set to 23 dBm.

The 2D AoA estimation is performed on the uplink using the estimators (32) and (33). The positioning is derived from the WLS estimator (39), incorporating the link quality metrics defined in (34), (35) and (36). Where indicated, the angular pre-filtering described in (44) is applied with a threshold of $T_r = 60°$.

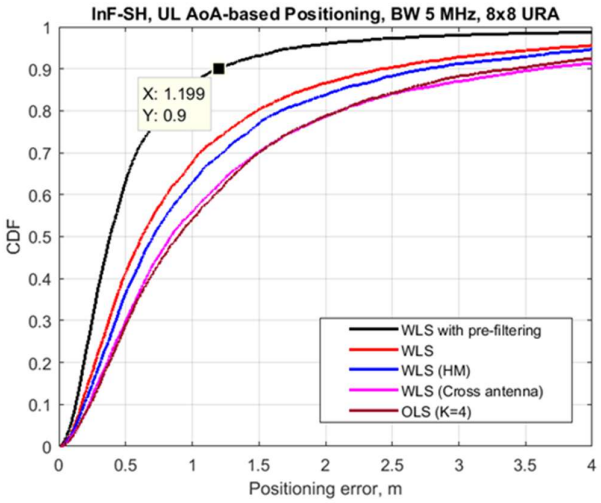

Figure 6. CDF of the horizontal positioning error for the 3D InF-SH scenario (5 MHz bandwidth, 8x8 URA).

As illustrated in Figure 6, the baseline approach utilizing the WLS estimator (39) with the link quality metric (36) without the additional angular pre-filtering (44) provides acceptable positioning accuracy (red curve). Specifically, the $90th$ percentile of the positioning error is below 2.4 m, which

 doi:10.20944/preprints202604.0043.v1

fulfills the requirements for commercial use cases specified in [4]. Furthermore, it is expected that positioning performance could be enhanced by utilizing a larger URA configuration.

If only the metric (34) corresponding to the horizontal plane is considered, the positioning error at the 90*th* percentile increases to 2.8 m (blue curve). Consequently, it is evident that the combination of metrics from both the horizontal and vertical planes, as defined in (36), provides a significant performance benefit.

It is important to note that 2D AoA measurements can also be performed using an antenna array consisting of only a single row and a single column. Such a configuration, known as a cross antenna, may be more attractive from an implementation standpoint than a full URA. However, this simplification leads to a notable reduction in positioning accuracy (magenta curve). Specifically, the 90*th* percentile of the positioning error increases to approximately 3.6 m.

The presented results demonstrate that the WLS approach significantly outperforms the OLS approach. When rigid selection is applied to the $K = 4$ best links, the positioning error at the 90*th* percentile is approximately 3.4 m (brown curve). This performance is comparable to that of the WLS estimator using a cross antenna and is notably inferior to the baseline WLS performance that utilizes the full set of links.

In conclusion, the performance of the baseline approach is significantly improved by the additional pre-filtering (44). Specifically, applying a threshold of $T_r = 60°$ reduces the 90*th* percentile positioning error to approximately 1.2 m (black curve). This level of accuracy surpasses the requirements for commercial use cases and closely approaches the stringent targets for industrial use cases [4].

The proposed method enables UE positioning in 3D space. Consequently, the overall system performance is determined by both the horizontal and vertical accuracy. Figure 7 illustrates the vertical positioning accuracy obtained under the simulation parameters outlined at the beginning of this section.

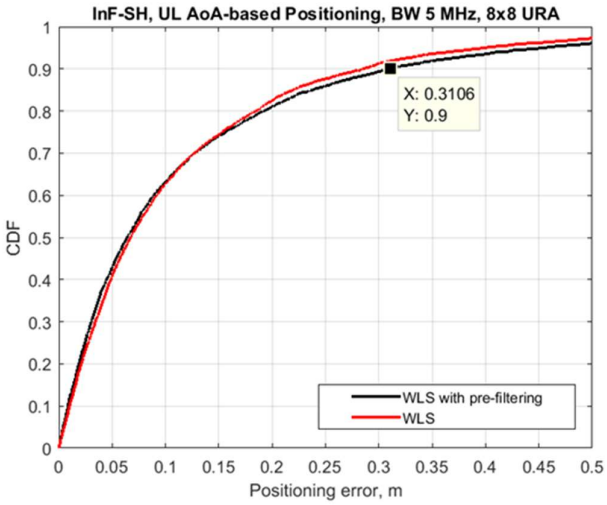

Figure 7. CDF of the vertical positioning error for the 3D InF-SH scenario (5 MHz bandwidth, 8x8 URA).

The results demonstrate that the proposed positioning method provides a highly accurate estimate of the UE height. Unlike the horizontal positioning results, the additional pre-filtering (44) has a negligible impact on vertical performance. This can be explained by the specific geometry of the simulated deployment, which prevents the occurrence of zenith angles near π (the array end-fire). Consequently, the achieved vertical positioning accuracy meets the requirements for both commercial and industrial use cases.

 doi:10.20944/preprints202604.0043.v1

4. Conclusions

5G indoor deployments are characterized by dense multipath conditions. For bandwidth-limited network entities such as RedCap UEs, these conditions hinder the application of conventional 5G positioning methods based on time-domain ranging (e.g., ToA and TDoA). A limited bandwidth prevents the proper resolution of direct and indirect paths, resulting in a drastic degradation of time-domain positioning performance. Consequently, the achieved accuracy may fail to satisfy specified requirements, necessitating the consideration of alternative approaches. Among these, methods based on AoA measurements are recognized for their robust performance in narrow-bandwidth scenarios.

In this paper, a comprehensive AoA-based positioning method is proposed, encompassing algorithms for 1D and 2D AoA estimation as well as a WLS-based localization framework for both 2D and 3D physical space. The enabling feature of this method is a link quality metric that facilitates high-precision indoor positioning. This metric is generated inherently during the 1D and 2D AoA estimation procedures, demonstrating the feasibility of standalone AoA-based 3D positioning.

While AoA-based positioning requires TRPs to be equipped with antenna arrays, these arrays primarily serve communication purposes. This work demonstrates that they can provide significant secondary benefits for localization. Furthermore, although 3D positioning can be achieved with simpler cross antenna arrays, the implementation of URAs is shown to be superior for ensuring accuracy. Simulation results indicate that the positioning requirements for RedCap UEs can be satisfied even in challenging InF scenarios, providing a robust alternative to bandwidth-constrained time-domain methods.

As a direction for future research, the proposed framework can be integrated into a hybrid localization solution. In particular, the obtained UE coordinates may serve as an initial estimate for high-precision carrier-phase positioning. Furthermore, the framework can be extended to other bandwidth-limited network entities, such as Ambient IoT (A-IoT) tags.

Author Contributions: Conceptualization, I.A., A.P. and S.H.; methodology, I.A. and A.P.; software, I.A. and A.P.; validation, S.H.; writing - original draft preparation, I.A. and A.P.; writing - review and editing, S.H. and H.K.; project administration, S.H. All authors have read and agreed to the published version of the manuscript.

Funding: This research received no external funding.

Institutional Review Board Statement: Not applicable.

Informed Consent Statement: Not applicable.

Data Availability Statement: The data presented in this study are available within the article.

Conflicts of Interest: The authors declare no conflicts of interest.

Abbreviations

The following abbreviations are used in this manuscript:

AoA	Angle of Arrival
A-IoT	Ambient Internet of Things
BW	Bandwidth
CP	Carrier Phase
eMBB	Enhanced Mobile Broadband
LoS	Line of Sight
ML	Maximum Likelihood
mMTC	Massive Machine-Type Communications
OFDM	Orthogonal Frequency-Division Multiplexing
OLS	Ordinary Least Squares
RedCap	Reduced Capability
RSS	Received Signal Strength

 doi:10.20944/preprints202604.0043.v1

TDoA	Time Difference of Arrival
ToA	Time of Arrival
TRP	Transmission and Reception Point
URLLC	Ultra-Reliable Low Latency Communications
UE	User Equipment
UL	Uplink
ULA	Uniform Linear Array
URA	Uniform Rectangular Array
WLS	Weighted Least Squares

References

1. Mogyorósi, F.; Revisnyei, P.; Paši'c, A.; Papp, Z.; Törös, I.; Varga, P.; Paši'c, A. Positioning in 5G and 6G Networks—A Survey. *Sensors* **2022**, 22, 4757. https://doi.org/10.3390/s22134757
2. Kim Geok, T.; Zar Aung, K.; Sandar Aung, M.; Thu Soe, M.; Abdaziz, A.; Pao Liew, C.; Hossain, F.; Tso, C.P.; Yong, W.H. Review of Indoor Positioning: Radio Wave Technology. *Appl. Sci.* **2021**, 11, 279. https://doi.org/10.3390/app11010279
3. A Glimpse into RedCap NR devices. Available online: https://www.3gpp.org/technologies/nr-redcap-glimpse (accessed on 25.03.2026).
4. 3GPP TR 38.859 V1.0.0 (2022-12) Study on expanded and improved NR positioning. Available online: https://portal.3gpp.org/desktopmodules/Specifications/SpecificationDetails.aspx?specificationId=3985 (accessed on 02.10.2025).
5. Report ITU-R SM.2211-2 Comparison of time-difference-of-arrival and angle-of-arrival methods of signal geolocation. Available online: https://www.itu.int/pub/R-REP-SM.2211 (accessed on 25.03.2026).
6. 3GPP TR 38.901 V17.0.0 (2022-04) Study on channel model for frequencies from 0.5 to 100 GHz. Available online: https://portal.3gpp.org/desktopmodules/Specifications/SpecificationDetails.aspx?specificationId=3173 (accessed on 25.03.2026).
7. Yan, J.; Tiberius, C.C.J.M.; Janssen, G.J.M.; Teunissen, P.J.G.; Bellusci, G. Review of range-based positioning algorithms. *IEEE Aerospace and Electronic Systems Magazine* **2013**, 28, 2-27. https://doi.org/10.1109/MAES.2013.6575420
8. Dun, H.; Tiberius, C.C.J.M.; Janssen, G.J.M. Positioning in a Multipath Channel Using OFDM Signals With Carrier Phase Tracking. *IEEE Access* **2020**, 8, 13011-13028. https://doi.org/10.1109/ACCESS.2020.2966070
9. Widdison, E.; Long, D.G. A Review of Linear Multilateration Techniques and Applications. *IEEE Access* **2024**, 12, 26251-26266. https://doi.org/10.1109/ACCESS.2024.3361835
10. R&S Introduction into Theory of Direction Finding. Available online: https://cdn.everythingrf.com/live/direction-finding-rs-wp-erf.pdf (accessed on 25.03.2026).
11. Bartlett, M.S. Periodogram Analysis and Continuous Spectra. *Biometrika* **1950**, 37, 1–16. https://doi.org/10.2307/2332141
12. Capon, J. High-resolution frequency-wavenumber spectrum analysis. *Proceedings of the IEEE* **1969**, 57, 1408-1418. https://doi.org/10.1109/PROC.1969.7278
13. Schmidt, R. Multiple emitter location and signal parameter estimation. *IEEE Transactions on Antennas and Propagation* **1986**, 34, 276-280. https://doi.org/10.1109/TAP.1986.1143830
14. Roy R.; Paulraj A.; Kailath, T. Estimation of Signal Parameters via Rotational Invariance Techniques – ESPRIT. In Proceedings of the MILCOM 1986 - IEEE Military Communications Conference: Communications-Computers: Teamed for the 90's, Monterey, CA, USA, 1986, pp. 41.6.1-41.6.5. https://doi.org/10.1109/MILCOM.1986.4805850
15. Stoica, P.; Nehorai, A. MUSIC, maximum likelihood, and Cramer-Rao bound. *IEEE Transactions on Acoustics, Speech, and Signal Processing* **1989**, 37, 720-741. https://doi.org/10.1109/29.17564
16. Ren, Q. S.; Willis, A.J. Extending MUSIC to single snapshot and on line direction finding applications. In Proceedings of the Radar 97 (Conf. Publ. No. 449), Edinburgh, UK, 1997, pp. 783-787. https://doi.org/10.1049/cp:19971783

 doi:10.20944/preprints202604.0043.v1

17. Tonello, A. M.; Inserra, D. Radio positioning based on DoA estimation: An implementation perspective. In Proceedings of the 2013 IEEE International Conference on Communications Workshops (ICC), Budapest, Hungary, 2013, pp. 27-31. https://doi.org/10.1109/ICCW.2013.6649195
18. Godara, L.C. *Handbook of Antennas in Wireless Communications (Electrical Engineering & Applied Signal Processing Series)*, 1st ed., CRC Press, 2001
19. Jansson, M.; Stoica, P. Analysis of forward-only and forward-backward sample covariances. In Proceedings of the 1999 IEEE International Conference on Acoustics, Speech, and Signal Processing (ICASSP99), Phoenix, AZ, USA, 1999, pp. 2825-2828 vol.5, https://doi.org/10.1109/ICASSP.1999.761350
20. Pillai, S.U.; Kwon, B.H. Forward/backward spatial smoothing techniques for coherent signal identification. *IEEE Transactions on Acoustics, Speech, and Signal Processing* **1989**, 37, 8-15. https://doi.org/10.1109/29.17496
21. Xiao, M.; Duan, Z.; Yang, Z. A Weighted Forward-Backward Spatial Smoothing DOA Estimation Algorithm Based on TLS-ESPRIT. *IEICE Transactions on Information and Systems* **2021**, E104.D, 881-884. https://doi.org/10.1587/transinf.2020EDL8144
22. Wan, F.; Zhu, W.-P.; Swamy, M.N.S. A Frequency-Domain Correlation Matrix Estimation Algorithm for MIMO-OFDM Channel Estimation. In Proceedings of the 2008 IEEE 68th Vehicular Technology Conference, Calgary, AB, Canada, 2008, pp. 1-5. https://doi.org/10.1109/VETECF.2008.72
23. Penrose, R. On best approximate solutions of linear matrix equations. *Mathematical Proceedings of the Cambridge Philosophical Society* **1956**, 52(1), 17-19. https://doi.org/10.1017/S0305004100030929
24. Grossman, W.D. Novel Line-of-Sight Three-Dimensional Triangulation Algorithm for Stationary Targets. *Journal of Guidance, Control, and Dynamics* **2018**, 41. https://doi.org/10.2514/1.G003204